BMC Urology

RESEARCH

Open Access

A prognostic model based on necroptosis-related genes for prognosis and therapy in bladder cancer

Zeyi Wang[1†], Zhengnan Huang[2†], Xiangqian Cao[3†], Fang Zhang[3], Jinming Cai[3], Pengfei Tang[1], Chenkai Yang[3], Shengzhou Li[3], Dong Yu[4*], Yilin Yan[5*] and Bing Shen[1,5*]

Abstract

Bladder cancer, one of the most prevalent malignant cancers, has high rate of recurrence and metastasis. Owing to genomic instability and high-level heterogeneity of bladder cancer, chemotherapy and immunotherapy drugs sensitivity and lack of prognostic markers, the prognosis of bladder cancer is unclear. Necroptosis is a programmed modality of necrotic cell death in a caspase-independent form. Despite the fact that necroptosis plays a critical role in tumor growth, cancer metastasis, and cancer patient prognosis, necroptosis-related gene sets have rarely been studied in bladder cancer. As a result, the development of new necroptosis-related prognostic indicators for bladder cancer patients is critical. Herein, we assessed the necroptosis landscape of bladder cancer patients from The Cancer Genome Atlas database and classified them into two unique necroptosis-related patterns, using the consensus clustering. Then, using five prognosis-related genes, we constructed a prognostic model (risk score), which contained 5 genes (ANXA1, DOK7, FKBP10, MAP1B and SPOCD1). And a nomogram model was also developed to offer the clinic with a more useful prognostic indicator. We found that risk score was significantly associated with clinicopathological characteristics, TIME, and tumor mutation burden in patients with bladder cancer. Moreover, risk score was a valid guide for immunotherapy, chemotherapy, and targeted drugs. In our study, DOK7 was chosen to further verify our prognosis model, and functional assays indicated that knockdown the expression of DOK7 could prompt bladder cancer proliferation and migration. Our work demonstrated the potential role of prognostic model based on necroptosis genes in the prognosis, immune landscape and response efficacy of immunotherapy of bladder cancer.

Keywords Bladder cancer, Necroptosis, Tumor immune microenvironment, Prognostic model, Immunotherapy, Chemotherapy

†Zeyi Wang, Zhengnan Huang and Xiangqian Cao contributed equally to this work.

*Correspondence:
Dong Yu
yudong615@126.com
Yilin Yan
yyl13338729720@163.com
Bing Shen
urodrshenbing@shsmu.edu.cn
[1] Department of Urology, Shanghai General Hospital of Nanjing Medical University, Shanghai 200080, China
[2] Department of Urology, Tongji Hospital, School of Medicine, Tongji University, Shanghai 200065, China
[3] Department of Urology, Shanghai General Hospital, Shanghai Jiaotong University School of Medicine, Shanghai 200080, China
[4] Department of Precision Medicine, Center of Translation Medicine, Naval Medical University, Shanghai 200082, China
[5] Department of Urology, Shanghai General Hospital, Shanghai Jiaotong University School of Medicine, Shanghai 200080, China

Background

Bladder cancer (BLCA), one of the most prevalent malignant cancers, has high rate of recurrence and metastasis, and there is a strong male predominance (male to female ratio 3:1) [1]. It is estimated that male BLCA new cases and deaths will rank fourth and eighth in the United States, respectively [1]. During 1975 to 2018, there is no significant change in the incidence of BLCA in men, but the incidence of other common tumors such as lung cancer decreased year by year [1]. BLCA present as muscle-invasive bladder cancer (MIBC), non-muscle-invasive bladder cancer (NMIBC) and metastatic diseases, approximately 75% of newly diagnosed BLCA patients present with NMIBC [2]. Radical cystectomy and cisplatin-based neoadjuvant chemotherapy are commonly options to treat BLCA especially MIBC. And new immunotherapy approaches are improving outcomes [3]. Yet, despite great progress in diagnosis and treatment, BLCA still shows a poor prognosis in high rates of metastasis and recurrence. The reason may be genomic instability and high-level heterogeneity of BLCA, chemotherapy and immunotherapy drugs sensitivity and lack of prognostic markers [4–6]. Therefore, there is an essential need to develop potential strategy to improve efficacy.

Necroptosis is a programmed modality of necrotic cell death in a caspase-independent form [7]. It has been reported that necroptosis is mainly mediated by receptor-interacting protein kinase 1 (RIPK1), RIPK3 and mixed lineage kinase domain-like pseudo kinase (MLKL), while necrostatin-1 (Nec-1) inhibits it [8]. Different with apoptosis, morphological features of necroptosis are typified as cell membrane rupture, organelle swelling and increasingly translucent cytoplasm [9, 10]. With the rupture of plasma membrane, cell contents are released which could lead to the exposure of damage-associated molecular patterns (DAMPs) and powerful inflammatory responses [11]. The dual-effects of necroptosis on cancer have been proven [12]. On the one hand, with the downregulation of necroptotic factors, it could cause a worse prognosis [13–15]. On the other hand, the upregulation of necroptotic factors also could lead to a worse prognosis and promote oncogenesis [16, 17]. Chemotherapy failure is a hard but common problem, and drug resistance induced by apoptosis plays a major role in it [12, 18]. There are lot of reports that chemotherapeutic agents could trigger necroptosis in cancer [19, 20], so we believe induced necroptosis may provide an effective therapy strategy in anti-cancer. Furthermore, RIPK1 expression and NF-κB activation during necroptosis could play a role of anti-tumor immunity by activate $CD8^{+}$T cells [21, 22]. Thus, necroptosis may also be of vital potential in the prognosis and therapy of BLCA.

Herein, we used multi-omics analysis to analysis the differences between necroptosis-related patterns based on the expression patterns of necroptosis-related genes (NRGs). Next, to predict the OS of BLCA patients, a prognostic model was constructed and validated its prognostic accuracy. In addition, we also built a nomogram model to provide clinical BLCA patients with precise and stable prognostic forecasts. Mutation profile, immune cell infiltration and immunotherapeutic and chemotherapeutic efficacy were also explored. Our study may provide a prognosis predicter and novel therapeutic targets for BLCA patients.

Methods

Obtaining and processing data

The datasets we used were all publicly available. Data of clinical information, somatic mutation and gene expression were obtained from The Cancer Genome Atlas (TCGA) data portal (https://portal.gdc.cancer.gov/). Data of clinical information and gene expression from the GEO database (https://www.ncbi.nlm.nih.gov/geo/, GSE13507) were used as an external test set. Next, in order to normalize the raw expression data, we used Robust Multiarray Average [23]. We obtained 74 NRGs from previous study [24]. Immunohistochemical (IHC) staining of DOK7 between BLCA and normal tissues were directly visualized by HPA (https://www.proteinatlas.org) [25].

Consensus clustering

In our study, we used consensus clustering to classify TCGA-BLCA cohort based on the expression of prognosis-related NRGs mRNA [26]. According to methods of previous study [27], the ideal cluster number was found to be $k=2$. The classification was verified by PCA based on the expression of prognosis-related NRGs mRNA of TCGA-BLCA cohort.

Tumor immune microenvironment evaluation

ssGSEA, CIBERSORT, and ESTIMATE were used in R to evaluate the TIME status of each BLCA sample. The enrichment scores of immune functions and immune cells were quantified using ssGSEA. ESTIMATE was applied for assess of the stromal, ESTIMATE and immune score. 22 tumor-infiltrating immune cells (TIICs) were valued by CIBERSORT algorithm.

Functional enrichment analysis of DEGs between necroptosis-related patterns

After consensus clustering, we examined the distinction of biological pathways of different expression gene set (DEGs) between necroptosis-related patterns through KEGG [28] and GO and pathway enrichment analyses.

The GO terms were in the cellular component (CC), biological process (BP) and molecular function categories (MF).

Establishment and validation of the prognostic model

We obtained the coefficient and selected the minimum criteria threshold for further screening 7 genes using LASSO Cox regression analysis. Eventually, the stepwise regression analysis provided a more practical and optimal model with five genes. In addition, the risk score formula was as follows:

$$Risk\ score = \sum_{n=1}^{i} \left(exp\ Genei \times coefficient\ Genei\right)$$

Based on the formula, we chose the mean value of risk score to divide TCGA-BLCA cohort into high- and low-risk groups. Next, the prognostic model's prediction ability was evaluated using the receiver ROC curve and Kaplan–Meier analysis. The GSE13507 datasets used the same approaches to validate the model.

Calculation of tumor microenvironment cell infiltration

XCELL, MCPCOUNTER, CIBERSORT, TIMER, EPIC, QUANTISEQ, and CIBERSORT-ABS were utilized to assess the relative proportions of infiltrating immune cells [29]. Spearman's rank correlation analysis was used when groping the correlation between the immune infiltrated cells and the risk score.

Evaluation of chemotherapy and immunotherapy drugs' efficacy

The pRRophetic software package was used to calculate the half-maximal inhibitory concentration (IC50) values of commonly used chemotherapy and immunotherapy drugs.

Cell culture and transfection

The human bladder cancer cell line 5637 was bought from the Cell Bank of Type Culture Collection of Chinese Academy of Sciences (Shanghai, China) and cultured in RPMI1640 supplemented with 10% FBS and penicillin–streptomycin (100 U/mL) in a humidified atmosphere of 5% CO2 at 37 °C. For the knockdown assay, small interfering RNA targeting DOK7 (siDOK7) was applied, and scramble siRNAs (siNC) as the negative control. The siRNA sequences targeting DOK7 was as follows: DOK7 siRNA sequence 5′-CUGGUCUACAAGGACAAGUTT-3′; siNC (noncoding control): 5′-UUCUCCGAACGU GUCACG U-3′.

Cell counting assay-8(CCK-8), wound healing assay and transwell migration assay

CCK8 assay (MCE, American) was used to analyze cell proliferation. 1×10^3 cells were cultured in 96-well plates for 24 h, 48 h and 72 h. Then, after incubation, 10 μL of CCK8 reagent was added into every well of 96-well plates and incubated for 2 h. After incubation of CCK8 reagent, we measured the OD value at 450 nm.

For the wound healing assay, the cells were plated in six-well plates, and cultured until 90% confluent. The confluent monolayer was wounded with a 200-μL pipette tip, and the unattached cells were removed. The scratches were observed at 0 h and 24 h after incubation of the monolayers in the FBS-free medium.

For migration assay, 1×10^4 bladder cancer cells were seeded on the upper 24-well transwell chambers (Corning) and culture for 24 h. After incubation, the cells move to the bottom of the 24-well chamber, followed by fixing with 4% formaldehyde and dyeing with crystal violet reagent.

Statistical analysis

All statistical analyses were performed using the R software (version 4.1.2). The Wilcoxon rank-sum test, paired samples *t*-test, and Kruskal–Wallis test were employed to validate the statistical difference between two groups or more than two groups, respectively. The correlation coefficients between tumor mutation burden (TMB), immune checkpoint genes (ICGs) expression, and risk score were calculated by Spearman's correlation analysis. P value < 0.05 was defined as a statistically significant standard.

Results

Consensus clustering of necroptosis-related patterns in TCGA-BLCA cohort

Using univariate COX regression, we selected 11 prognosis-related NRGs from 74 NRGs (Fig. 1A). Based on 11 prognosis-related NRGs, we performed consensus clustering on TCGA-BLCA cohort. According to cophenetic coefficients, $k = 2$ was found to be the ideal cluster (Fig. 1B, C). Ultimately, we identify two different necroptosis-related patterns named cluster A and cluster B. After clustering, Kaplan–Meier analysis demonstrated that cluster A has significantly better survival time than cluster B (Fig. 1D). Next, we performed PCA to show the distinction between cluster A and cluster B at the 11 prognosis-related NRGs transcription level (Fig. 1E). The transcription profile of 11 prognosis-related NRGs was presented as heatmap (Fig. 1F). As Fig. 1G showed that the distribution of age, grade, pathologic stage, T stage and N stage were significantly

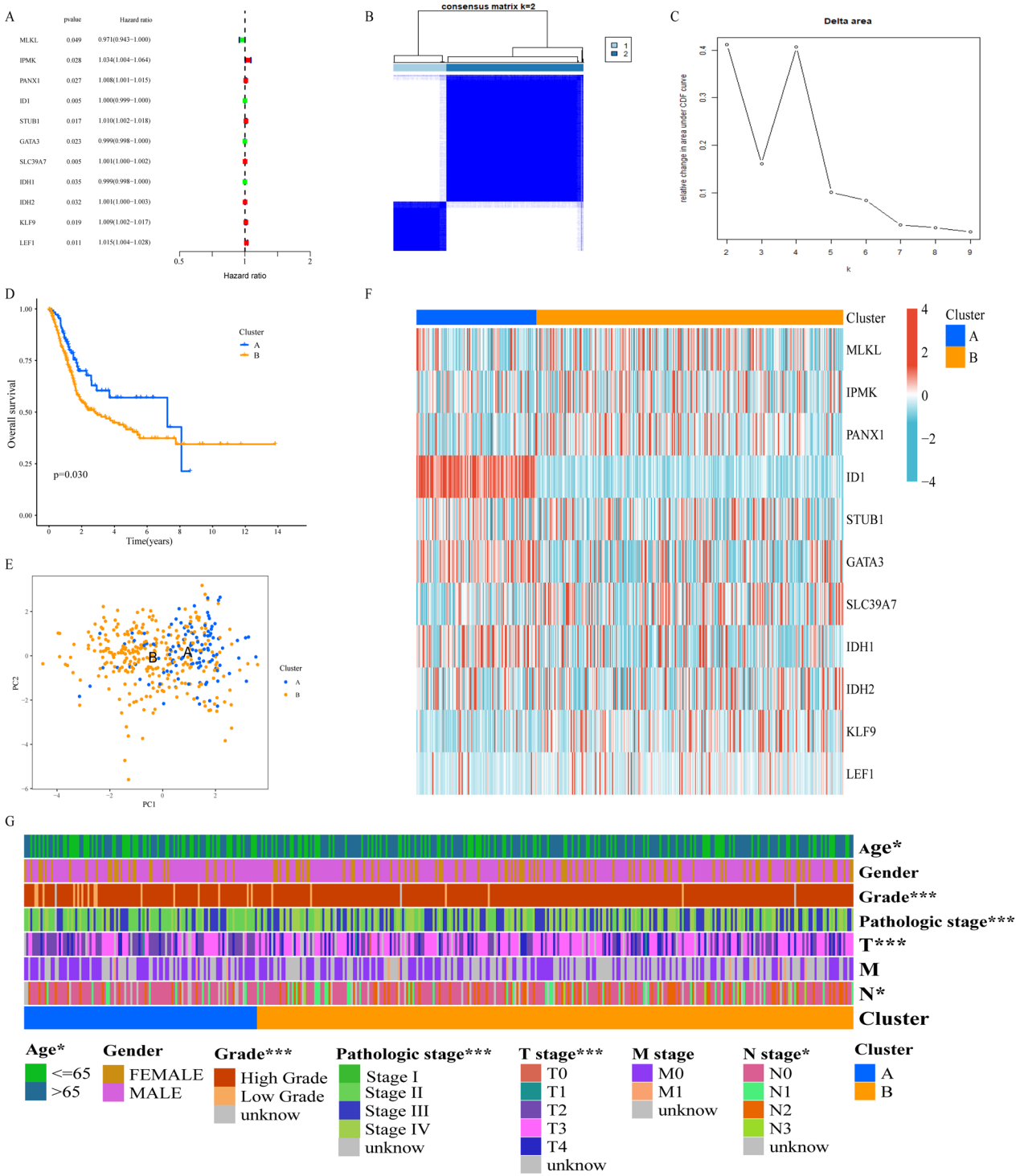

Fig. 1 Consensus Clustering of Necroptosis-Related Patterns in TCGA-BLCA cohort. **A** Prognosis-related NRGs selected by univariate COX regression analysis. **B** Consensus matrix heatmap defining two clusters (k = 2) and their correlation area. **C** Cumulative distribution function curve. Kaplan–Meier analysis (**D**) and PCA analysis (**E**) of necroptosis-related patterns. **F** NRGs with a prognosis-related expression profile. **G** Clinical relevance of necroptosis-related patterns. *$p < 0.05$; **$p < 0.01$; ***$p < 0.001$

distinct between cluster A and cluster B by chi-square test.

Tumor immune microenvironment of necroptosis-related patterns

By using GSEA analysis, we confirmed that cluster A has higher concentration in metabolism, while cluster B has a higher concentration in carcinogenic-related pathways and immune-related diseases (Fig. 2A, B). To distinguish the associations between tumor immune microenvironment and two subtypes, we first using ESTIMATE to calculated the tumor microenvironment composition (Fig. 2C). The StromalScore, ImmuneScore, and ESTIMATEScore of cluster A were all notably lower than those in cluster B. In addition, several immune checkpoints expression, including PDCD1, CD274,

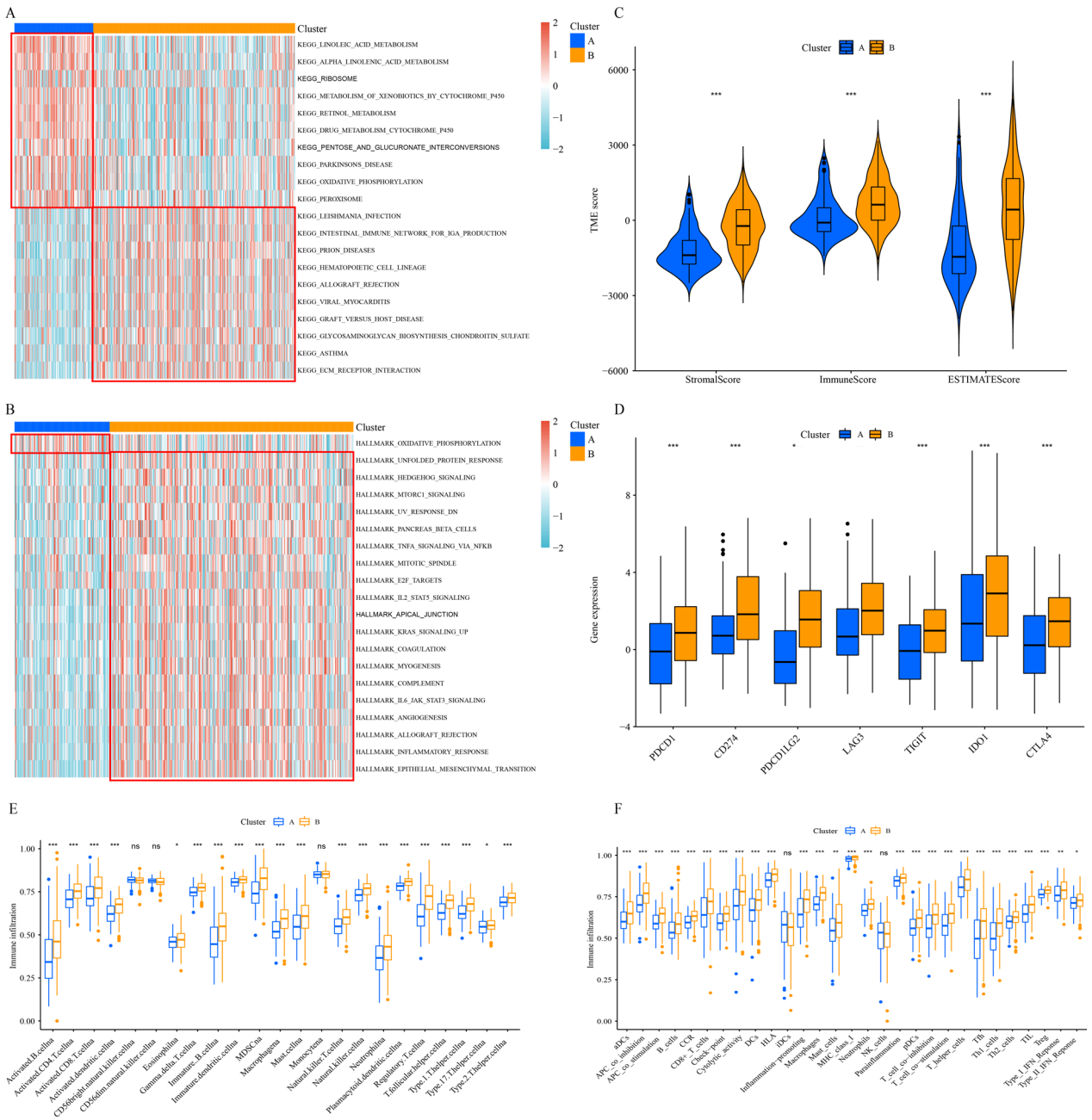

Fig. 2 Correlation between the tumor immune microenvironment and necroptosis-related patterns. Heatmap of GSEA analysis results based on KEGG gene set (**A**) and HALLMARK gene set (**B**). **C** A comparison of stromal, immune, and ESTIMATE scores. **D** Differential analysis of ICGs expression. **E** Infiltration of 23 TIICs in two necroptosis-related patterns. **F** Enrichment scores of immune-related functions in two necroptosis-related patterns. *$p < 0.05$; **$p < 0.01$; ***$p < 0.001$, ns = no significance

PDCD1LG2, IDO1, LAG3, TIGIT and CTLA4, were higher in cluster B (Fig. 2D). Moreover, the infiltration of B cells, eosinophilna, T cells, macrophages, dendritic cells and neutrophils in cluster B were notably higher than those in cluster A (Fig. 2E). Uniformly, almost all immune functions were highly expressed in cluster B (Fig. 2F).

Figure 3A showed the DEGs between necroptosis-related patterns by volcano plot. Functional enrichment analyses of DEGs between two subtypes were applicable to grope diversities the molecular diversity. GO analysis indicated that DEGs were mainly involved in positive regulation of cell activation and multiple immune-related biological processes (Fig. 3B). Cellular Components were mostly located in collagen—containing extracellular matrix, external side of plasma membrane and immunoglobulin complex (Fig. 3C). Molecular functions were mostly concentrated in antigen binding, extracellular matrix structural constituent and glycosaminoglycan binding (Fig. 3D). Consistently, the DEGs were related to several immune-related pathways, such as the chemokine signaling pathway, TGF-β signaling pathway and NF-κB signaling pathway (Fig. 3E).

Establishment and validation of the prognostic model in TCGA-BLCA cohort

Based on the necroptosis-related patterns and prognosis-related genes between two subtypes, we established a prognostic model to obtain a metrics that could correctly predict the clinical survival of BLCA patients. The minimum threshold for further screening 9 genes was determined using LASSO Cox regression analysis (Fig. 4A, B). After optimizing the model with stepwise regression analysis, only five genes remain: ANXA1, DOK7, FKBP10, MAP1B and SPOCD1. We also obtained a quantitative metrics: Risk score = (FKBP10 expression × 0.13145) + (MAP1B expression × 0.13152) + (ANXA1 expression × 0.16761) − (SPOCD1 expression × 0.14438) − (DOK7 expression × 0.14033). Based on the formula and the mean value of risk score, we divided patients into the high- and low-risk group. According to Kaplan–Meier analysis, the OS of BLCA patients in the low-risk group was significantly better than that of the high-risk group (Fig. 4C). Additionally, the AUCs for OS survival at 1, 3 and 5 years were 0.702, 0.697 and 0.671, respectively (Fig. 4D). Figure 4E, F showed that the proportion of deaths were positively associated with risk scores. The expression of SPOCD1 and DOK7 were negatively correlated with risk score, whereas FKBP10, MAP1B and ANXA1 were increased with the increasing of risk score (Fig. 4G).

Besides, we used GSE13507 as a test set to further validate the accuracy of risk score in BLCA patients. We used the same formula to quantify the samples in the test set and group them with the same cutoff values. Kaplan–Meier analysis indicated high risk score significantly correlated with poor OS (Fig. 4H). The AUCs for OS survival at 1, 3 and 5 years were 0. 723, 0. 662 and 0. 630, respectively (Fig. 4I). Risk score distribution, survival status and expression profile heatmaps showed similar tendencies to the training set (Fig. 4J–L). Hence, we believe that the prognostic model could be an accurate and effective risk factor for BLCA.

Clinical relevance of the prognostic model

We assessed the connection between clinicopathological parameters and risk score to further investigate the clinical relevance of the prognostic model. Just as Fig. 5A showed that patients older than 65 years scored higher than patients less than or equal to 65 years. And with the grade, pathologic stage, and TNM stages progressed, the risk

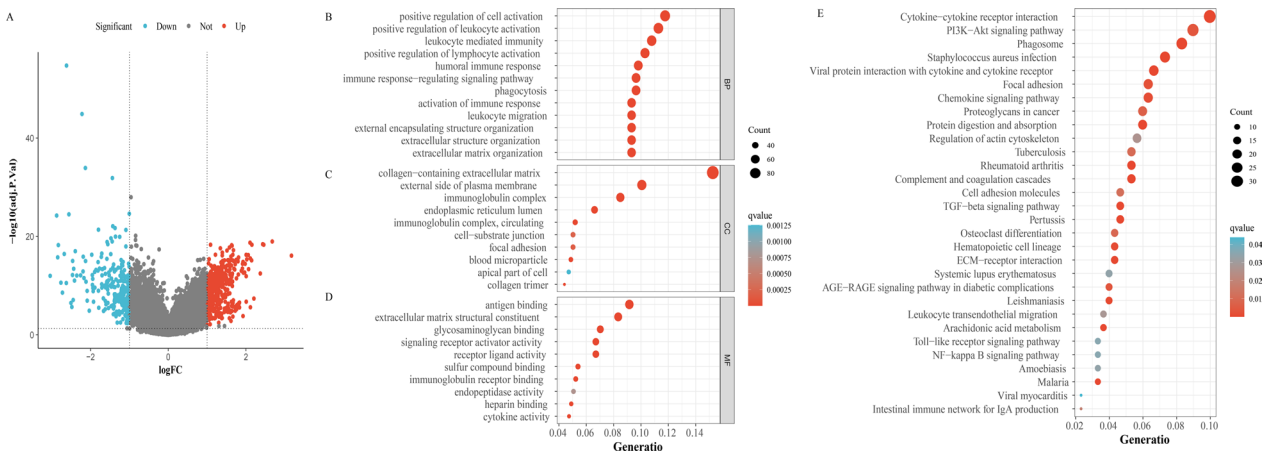

Fig. 3 Functional enrichment analyses of DEGs between necroptosis-related patterns. **A** DEGs between necroptosis-related patterns**.** Biological process (**B**), cellular component (**C**), molecular function (**D**), and KEGG pathways (**E**)

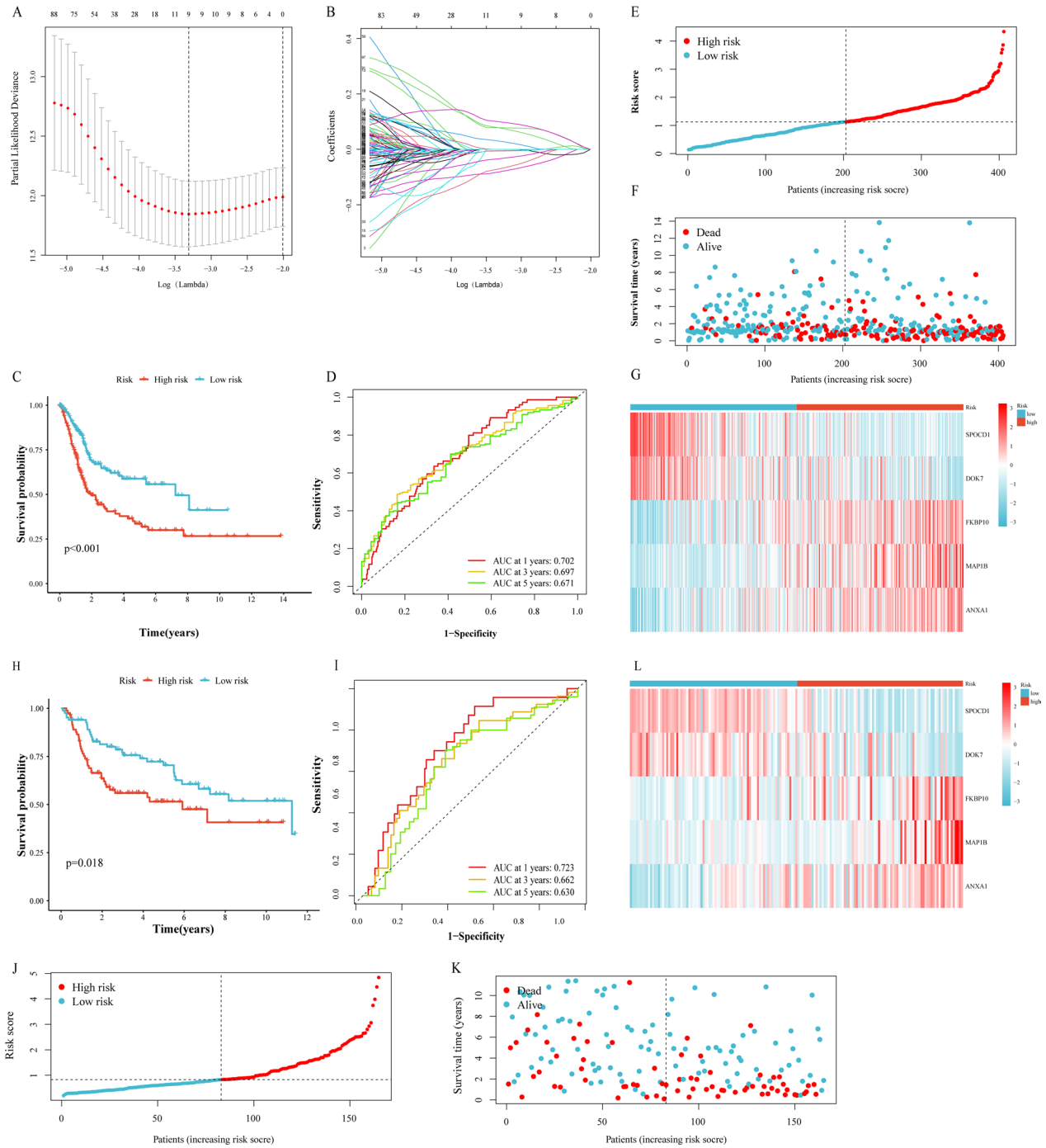

Fig. 4 Construction and validation of the prognostic model based on the TCGA-BLCA cohort and GSE13507. **A**, **B** LASSO COX regression analysis. Kaplan–Meier analysis (**C**), time-dependent ROC curve (**D**), risk score distribution (**E**), heatmap of survival statue (**F**), and heatmap of NRG expression profile (**G**) based on the TCGA-BLCA cohort. Kaplan–Meier analysis (**H**), time-dependent ROC curve (**I**), risk score distribution (**J**), heatmap of survival statue (**K**), and heatmap of NRG expression profile (**L**) based on the GSE13507

score increased significantly (Fig. 5B–F). But there was no statistical distinction between the gender groups (Fig. 5G).

Furthermore, we used univariate and multivariate Cox regression analysis to see if risk score was a reliable prognostic factor for BLCA patients. In univariate Cox regression analysis, age, pathological stage, T stage, N stage, and risk score were identified as risk factors (Fig. 5H). The risk score was subsequently validated using multivariate

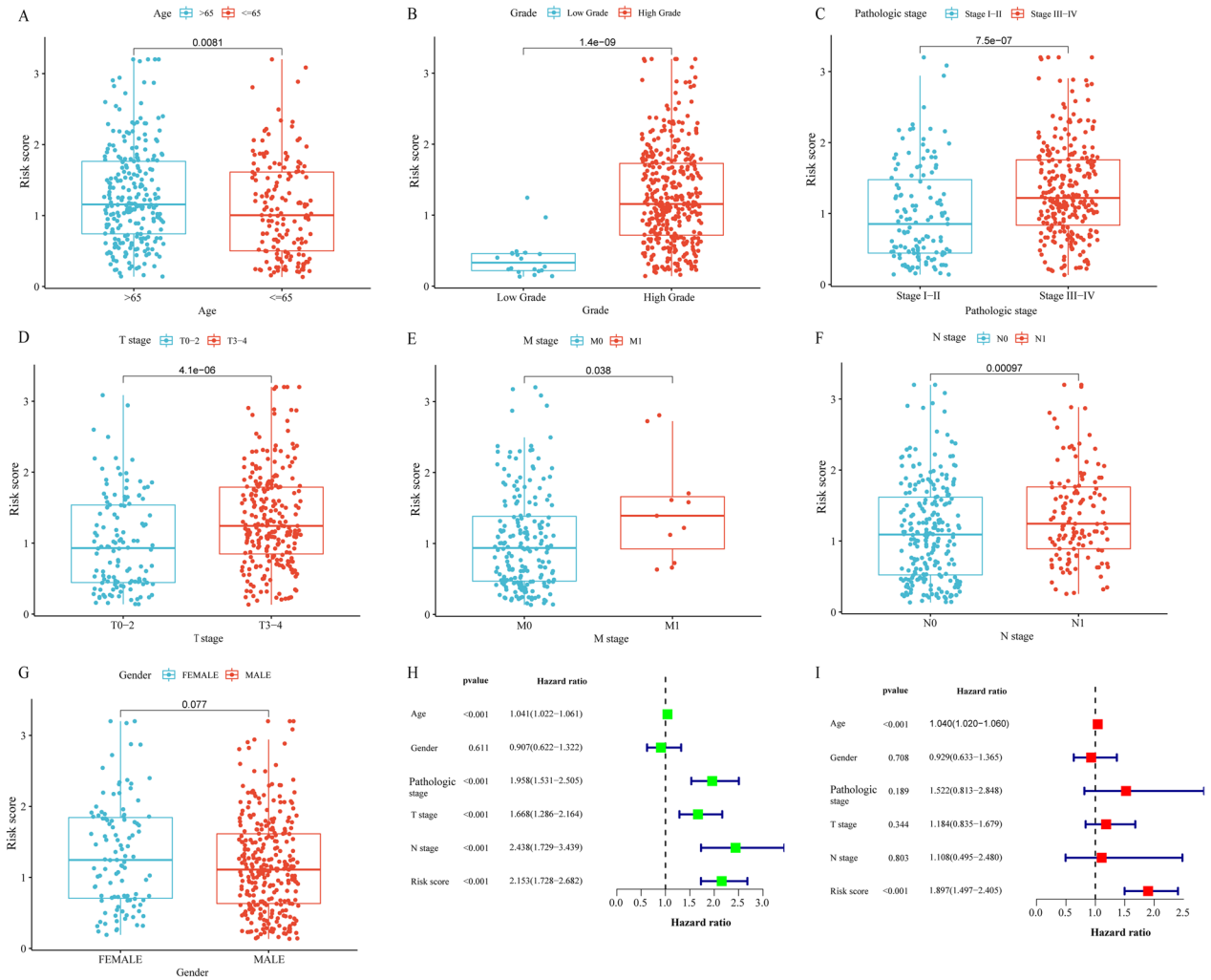

Fig. 5 Clinical relevance of the Prognostic model. **A–G** Risk score differences between risk score defined groups of clinicopathological parameters, including age (**A**), grade (**B**), pathologic stage (**C**), T stage (**D**), M stage (**E**), N stage (**F**) and gender (**G**). Univariate (**H**) and multivariate (**I**) Cox regression analysis of risk score and clinicopathological parameters. *$p < 0.05$; **$p < 0.01$; ***$p < 0.001$, ns = no significance

Cox regression analysis, indicating that it may be utilized as a reliable independent predictive indicator for BLCA patients (Fig. 5I).

Construction of a nomogram model based on the prognostic model

Based on the above results, patients of high- and low-risk group were assigned the corresponding scores, and the other predicters (N stage, gender, T stage, pathologic stage and age) were also assigned scores respectively. Based on that, we constructed a nomogram model (Fig. 6A). It was show that the 59 years old female patient we select belongs to the low-risk group, at T3N0 stages and pathologic stage III. The assigned scores of the patient were 35, 42, 57, 57, 68 and 69, respectively, with final overall scores of 328. Survival rates were 0.913, 0.759, and 0.707 after 1-, 3-, 5-year, respectively. Next, the calibration plots also confirmed the excellent predictive accuracy of the nomogram model (Fig. 6B).

Next, Fig. 6C presented the ROC curves of the nomogram and its constituent variables for OS. The AUCs of the nomogram and risk for predicting OS survival rate were 0.768 and 0.713, respectively. Consistently, DCA curves demonstrated that risk and nomograms have higher clinical application than pathological staging, age and gender in predicting patient OS (Fig. 6D).

Correlation between tumor immune microenvironment and the prognostic model

We further analyzed the correlation between TIME and prognostic model. Using the ESTIMATE algorithm, we first calculated the difference in TME score between

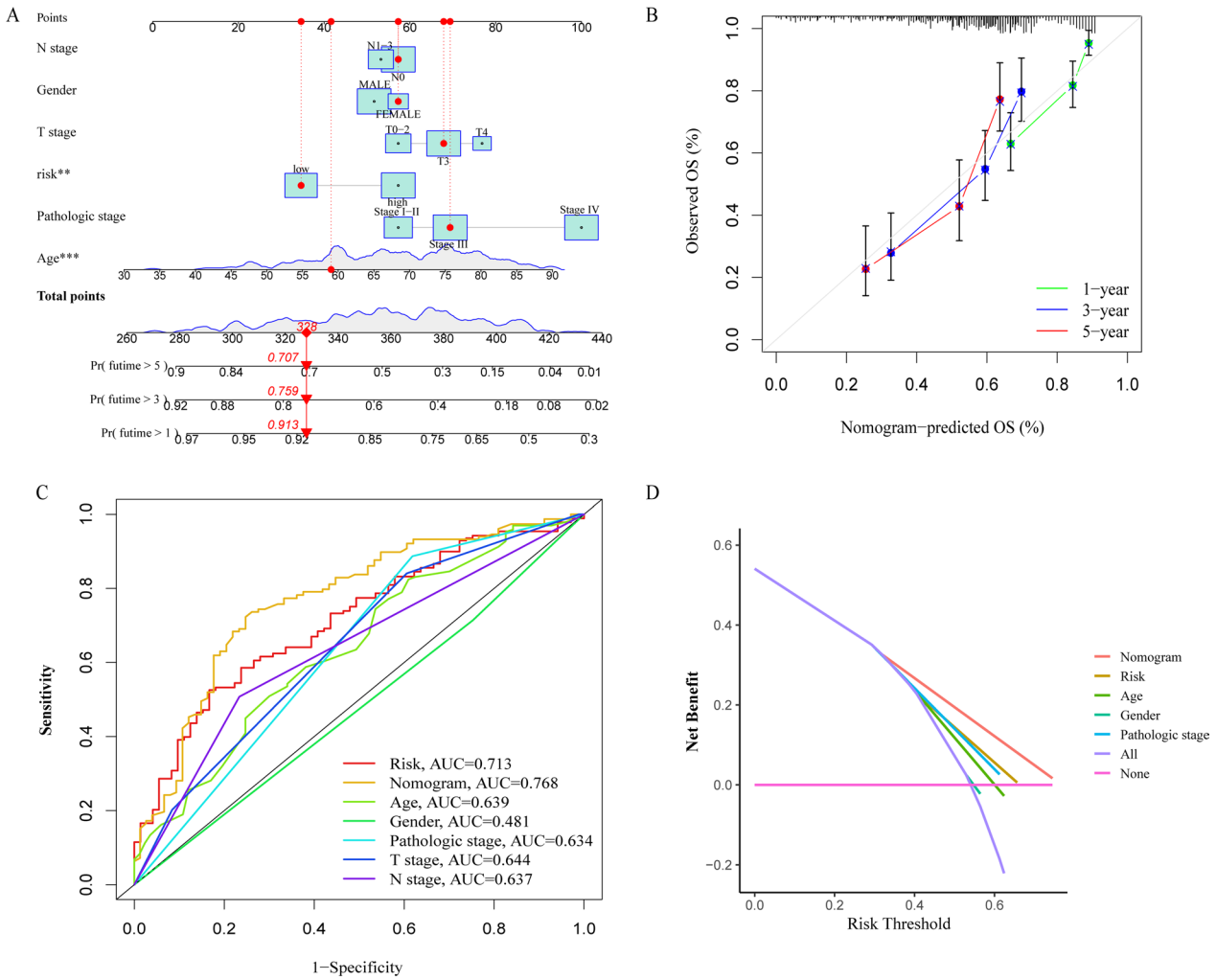

Fig. 6 Nomogram model construction. **A** Nomogram predicting the likelihood of OS in 1, 3, and 5 years. **B** Calibration curves for assessing the suitability of the nomogram model in 1, 3 and 5 years. **C** ROC curves of the nomogram, risk and its constituent variables (age, gender, pathologic stage, T stage, N stage) for predicting OS. **D** DCA curves

high- and low-risk groups (Fig. 7A). The Wilcoxon rank-sum test advised that StromalScore, ImmuneScore and ESTIMATEScore in the low-risk group are significantly lower compare to the high-risk group. The correlation between immune cells and risk score was calculated as well (Fig. 7B). ssGSEA suggested that the majority of immune-related functions were strongly concentrated in the high-risk group (Fig. 7C). Then, GSEA was utilized to investigate potential biological processes and signal pathways. Based on the KEGG gene set, we noticed the concentration level of high-risk group in cell adhesion molecules cams, ECM receptor interaction, cytokine-cytokine receptor interaction, hematopoietic cell lineage and neuroactive ligand receptor interaction (Fig. 7D). While the concentration level of low-risk group in drug metabolism-cytochrome P450, metabolism of xenobiotics by cytochrome p450, Pentose and glucuronate interconversions, Porphyrin and chlorophyll metabolism and steroid hormone biosynthesis (Fig. 7E).

Next, the CIBERSORT algorithm was applied to calculate the fraction of 22 TIICs in each TCGA-BLCA sample. A grouping histogram depicting the distribution of TIICs in BLCA (Fig. 8A). Then, we fund that the fractions of activated CD4 memory T cell, M0, M1 and M2 Macrophages were significantly higher in the high-risk group (Fig. 8B), while memory B cells, CD8 T cells, naïve CD4 T cells, follicular helper T cells (Tfh), regulatory T cells (Tregs), monocytes, resting and activated dendritic cells (DCs) were significantly higher in the low-risk group (Fig. 8B). Higher proportions of memory B cells and lower fractions of activated CD4 memory T cell, Tfh, CD8 T cells and resting DCs among these differently distributed TIICs were substantially linked with poor OS in BLCA patients (Fig. 8C–G). Hence, we

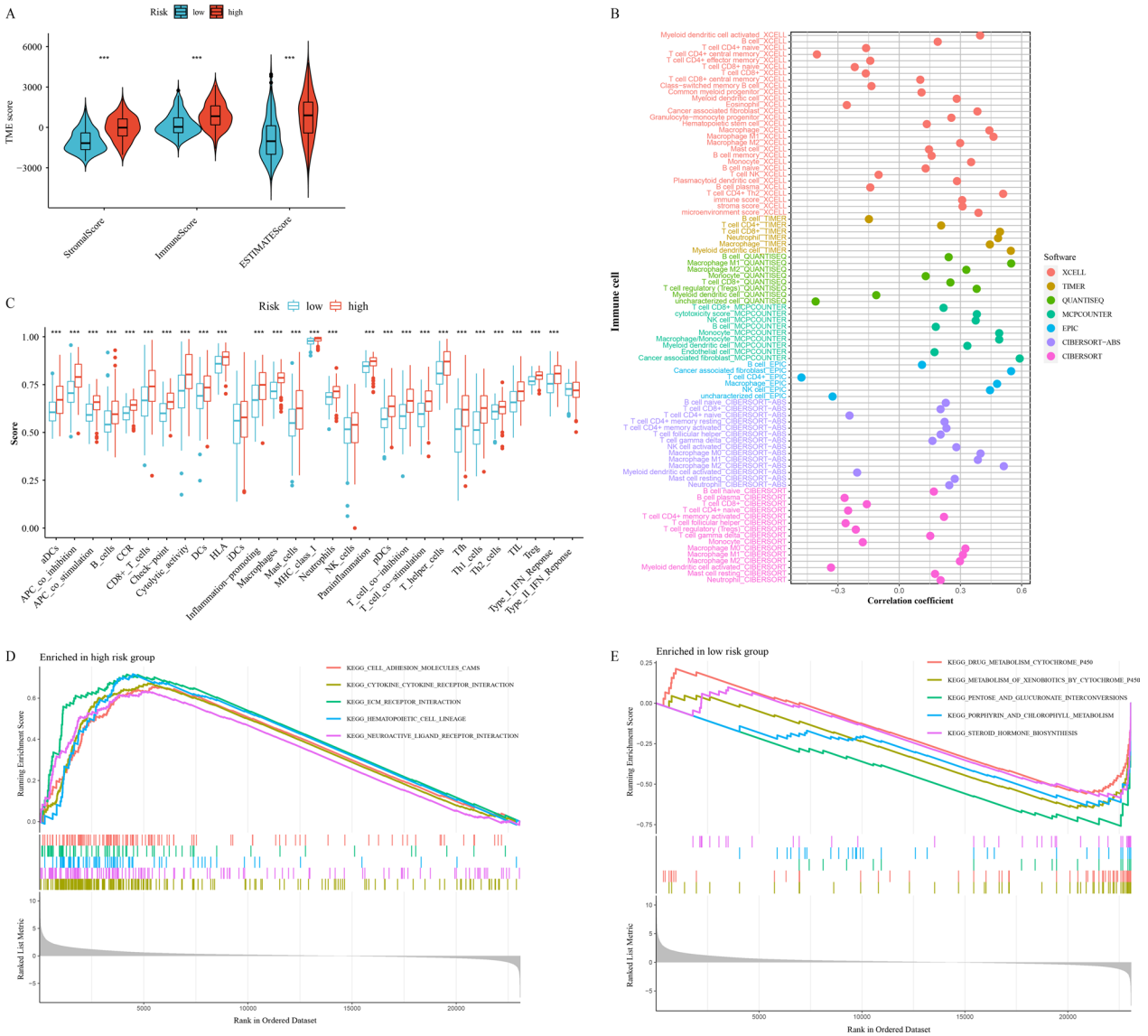

Fig. 7 Correlation between the prognostic model and tumor immune microenvironment. **A** A comparison of stromal, immune, and ESTIMATE scores. **B** The relationship between immune cells and risk Score. Each color represented a distinct algorithm. **C** Enrichment scores for immune-related functions in groups defined by risk scores. GSEA analyses based on KEGG in the high-risk group (**D**) and the low-risk group (**E**). *$p < 0.05$; **$p < 0.01$; ***$p < 0.001$, ns = no significance

believe necroptosis might regulate these TIICs to affect the prognosis of BLCA patients.

Correlation between the prognostic model and somatic mutation and drug sensitivity

There was a lot of evidence that tumorigenesis was associated with accumulation of gene mutations. Figure 9A, B revealed simple nucleotide variation of risk score groups in BLCA cases, suggesting that the 20 genes with the highest mutation rate in BLCA were TP53, TTN, KMT2D, MUC16, ARID1A, KDM6A, PIK3CA, SYNE1, RB1, FGFR3, HMCN1, KMT2C, RYR2, MACF1, EP300, FLG, FAT4, STAG2, ATM and OBSCN. Then, to split patients into low- and high-TMB groups, we determine the best TMB cutoff value. BLCA patients with lower TMB were associate with poorer OS (Fig. 9C). In addition, BLCA patients with lower TMB and higher risk scores have poorer OS survival probability, whereas BLCA patients with higher TMB and lower risk scores have greater OS (Fig. 9D).

In addition, we investigated potential correlations between ICGs expression and risk score. Figure 9E showed that risk score was significantly positively associated with the expression of PDCD1, CTLA4, POLE2,

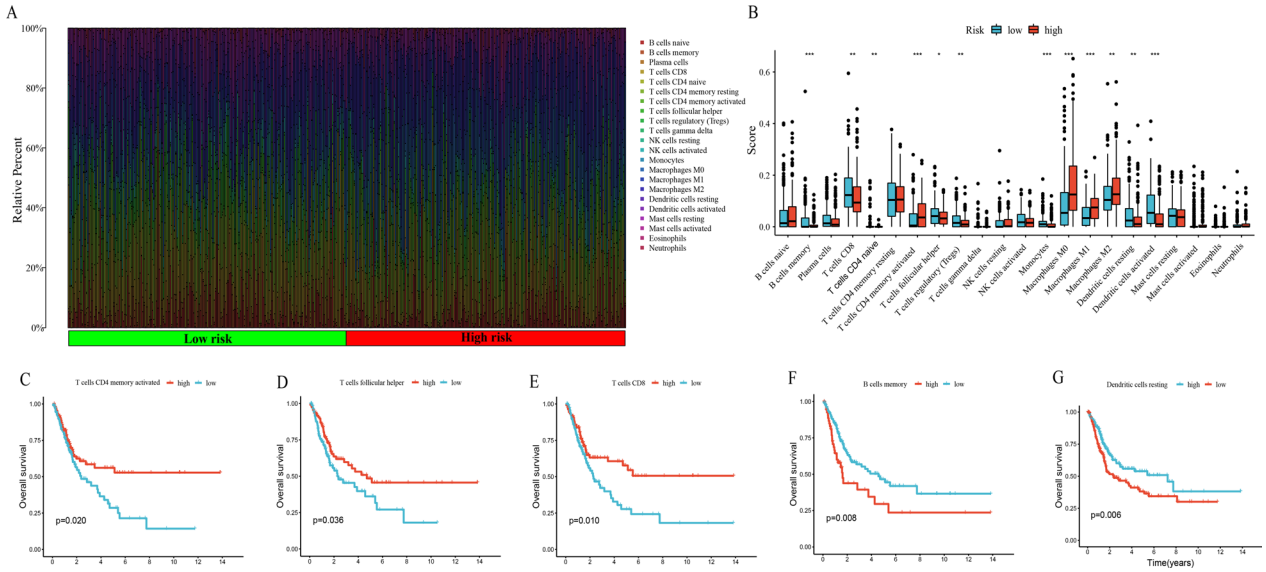

Fig. 8 Correlation between the fraction of 22 TIICs and the prognostic model. **A** Proportion of 22 TIICs in BLCA. **B** Differential analysis of 22 TIIC fractions between risk score-defined groups. **C**–**G** Association between the infiltration level of TIICs [activated CD4 memory T cells (**C**), follicular helper T cells (**D**), CD8T cells (**E**), memory B cells (**F**), resting dendritic cells (**G**)] and OS of BLCA patients. *$p < 0.05$; **$p < 0.01$; ***$p < 0.001$, ns = no significance

FEN1, MCM6, POLD3, CD274, MSH6, FAP and LOXL2. And the TIDE score was significantly lower in low-risk group (Fig. 9F). As a result of the abovementioned, immunotherapy was more likely to benefit BLCA patients in the high-risk group.

Next, we calculated IC50 values to predict risk score for chemotherapy and immunotherapy drugs. The IC50 value of doxorubicin, docetaxel, cisplatin, tipifarnib, sunitinib, sorafenib and pazopanib was notably lower in the high-risk group, suggesting that BLCA patients with high-risk score were more benefit from these drugs (Fig. 9G–M).

Functions of the identified biomarker in bladder cancer progression

Five genes in our prognostic model, ANXA1, MAP1B and SPOCD1 have been reported in bladder cancer, however DOK7 and FKBP10 has not been studied in bladder cancer [30–33]. There was reported that DOK7 could inhibit breast cancer cell invasion and migration ability via PI3K/PTEN/AKT pathway [34], and in our above results, the DEGs were related to PI3K/AKT signaling pathway. So, we chose DOK7 to further verify our prognostic model. According to the data of TCGA, patients who have higher expression of DOK7 have a better OS, and with the staging increase the expression of DOK7 has decreased (Fig. 10A, B). In addition, we investigated the protein expression of DOK7 in high grade tumor, low grade tumor and normal bladder tissues respectively by using the HPA dataset, and immunohistochemical staining indicated the positive staining intensity of DOK7 in normal bladder tissues as notably stronger than BLCA tissues. Moreover, tumor samples with a low pathological grade revealed stronger expression than tissues with a high grade by HPA (Fig. 10C).

Last, functional studies were performed by using small interfering RNAs (siRNAs) to knockdown of DOK7, and the results indicated that the knockdown of DOK7 could promote the cell proliferation and migration ability (Fig. 10D–F). All of the results were consistent with our prognostic model.

(See figure on next page.)

Fig. 9 Correlation between the prognostic model and somatic mutation and drug sensitivity. **A**, **B** Waterfall plots of 20 genes with the highest mutation rate in the high-risk group (**A**) and low-risk group (**B**). Kaplan–Meier analysis of TMB in BLCA patients based on TMB defined groups (**C**) and risk score with TMB-defined groups (**D**). **E** Correlation between expression of ICGs and risk score. **F** TIDE score. Correlation between the Prognostic model and IC_{50} values of chemotherapy and immunotherapy drugs, including doxorubicin (**G**), docetaxel (**H**), cisplatin (**I**), tipifarnib (**J**), sunitinib (**K**), sorafenib (**L**) and pazopanib (**M**)

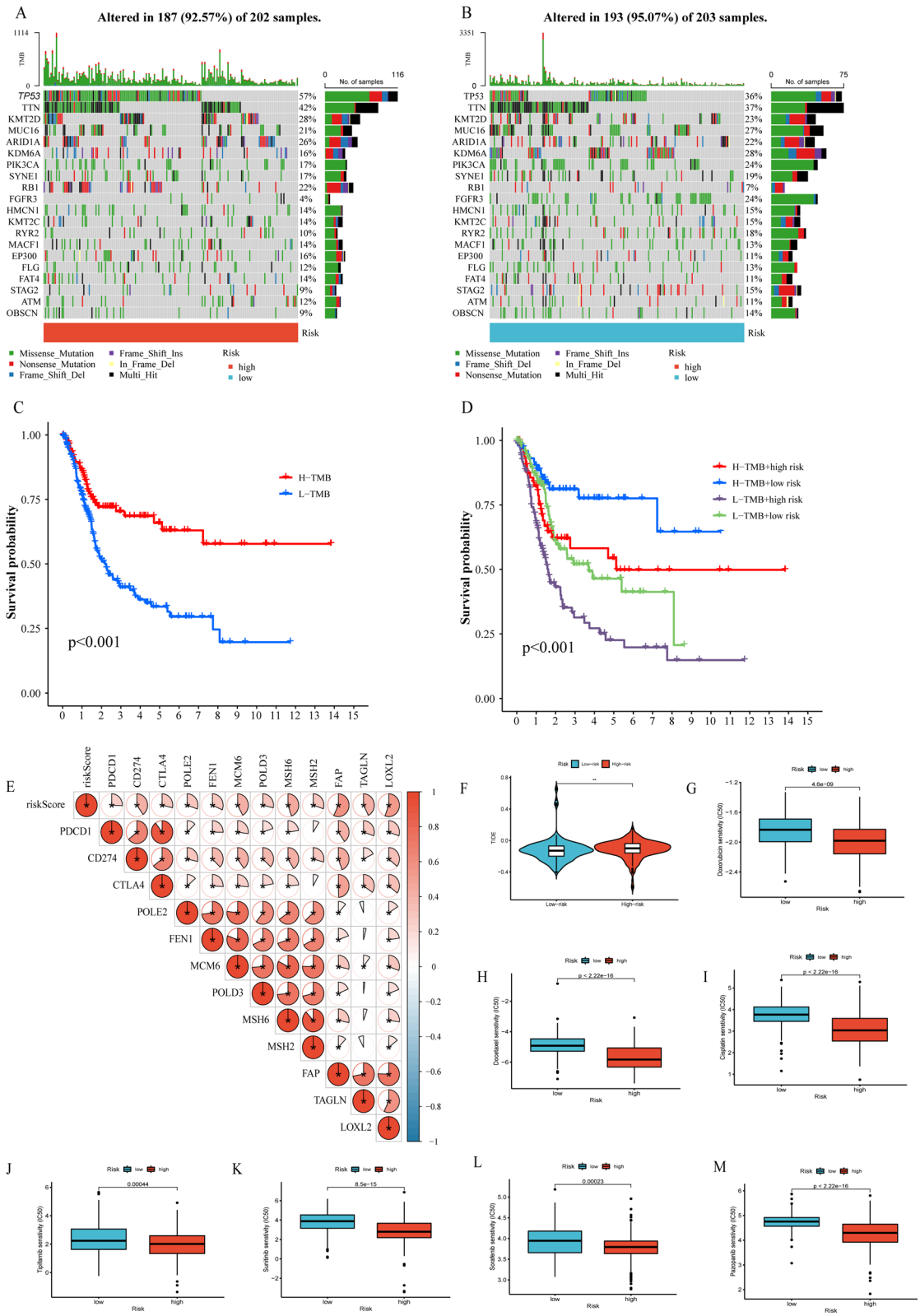

Fig. 9 (See legend on previous page.)

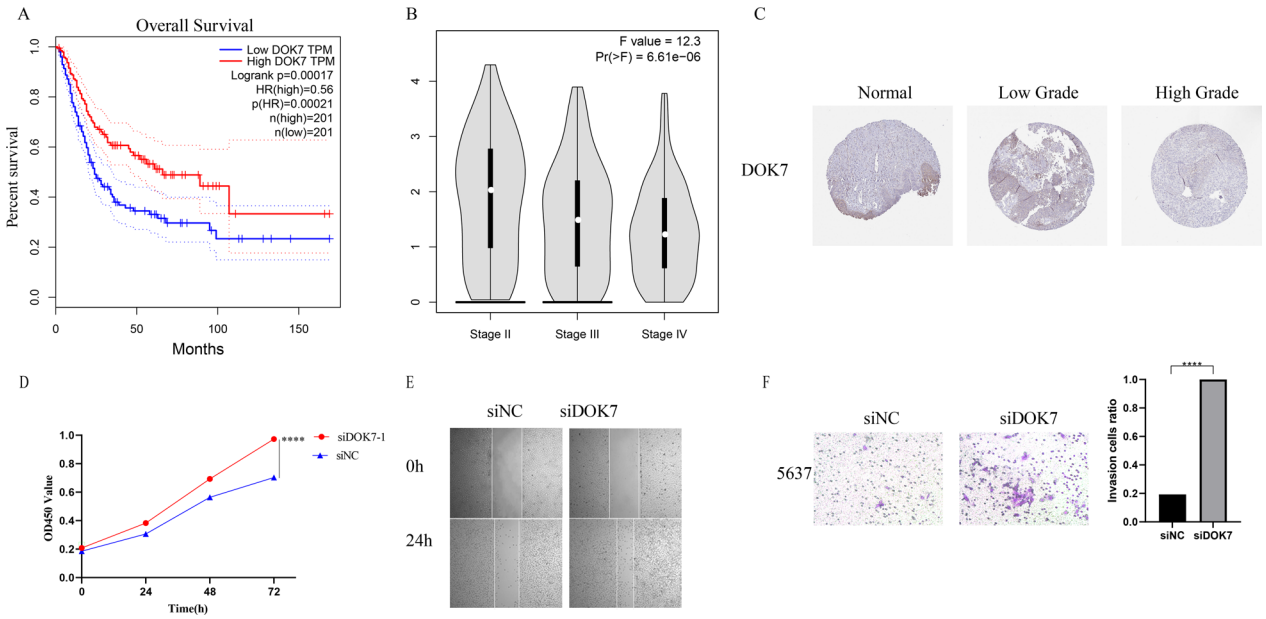

Fig. 10 Functions of the identified biomarker in bladder cancer progression. **A** Relationship between the expression level of DOK7 and OS in TCGA. **B** Relationship between the expression level of DOK7 and cancer stage in TCGA. **C** Immunohistochemical (IHC) analysis of DOK7 in normal bladder tissues and tumor tissues with different grades of malignancy. **D**–**F** CCK-8, wound healing and transwell migration assay for analyzing the effect of DOK7 knockdown on cell proliferation and migration

Discussion

Despite significant advancements in diagnosis and therapy, bladder cancer remains a serious clinical problem due to high rates of recurrence and metastasis [4]. As a result, optimizing therapy regimens to reduce BLCA patient mortality is critical.

There are several prognostic models about bladder cancer have been explored, and they classified bladder cancer with pyroptosis-related genes, ferroptosis-related genes, and neutrophil-related genes or m6A-immune-related lncRNA [35–38]. But our prognostic model is based on necroptosis-related genes in bladder cancer, and to predict the prognosis and treatment of bladder cancer.

In our study, by consensus clustering, we uncovered two necroptosis-related patterns using BLCA samples from the TCGA-BLCA. Cluster B has a much lower OS survival rate and a significantly higher percentage of patients in advanced clinicopathological stages. In addition, several immune checkpoints were discovered to be substantially expressed in Cluster B (PDCD1, CD274, IDO1, PDCD1LG2, LAG3, TIGIT and CTLA4). Furthermore, TME immune cell infiltration and biological pathway enrichment differ between these two necroptosis-related patterns. Cluster B was distinguished by significant levels of TME immune cell immersion and adaptive immunity activation in this pattern. Based on above results, we hypothesized that immune checkpoints genes expressed high-level could strengthen T cell activation and activate the immune pathway to weak the effects of tumor suppression and elimination [39], and we believed that necroptosis may has a critical role in BLCA's immune landscape regulation and may be a prognosis predictor.

Next, we established a prognostic model including five genes (ANXA1, DOK7, FKBP10, MAP1B and SPOCD1) to obtain a metrics that can forecast the clinical survival rate of BLCA patients accurately and effectively. A series of analyses indicated that BLCA patients in high-risk groups have poorer OS and prognosis event in the TCGA-BLCA cohort. And it was consistently verified in GSE13507 cohort. The risk score was subsequently validated using univariate and multivariate Cox regression analysis, indicating that it may be utilized as a reliable independent prognostic indicator for BLCA patients. ANXA1 is a member of annexins superfamily, and plays a role in inflammation regulation and can influence T cell proliferation [40, 41]. ANXA1 also could promotes the progression and drug resistance in bladder cancer [30, 42]. DOK7 is a docking protein correlate with tumor recurrent and an indicator of cancer risk [43–45]. Overexpression of FKBP10 is find to boost cancer progression by restrict antitumor immunity or activate tumor-related signaling pathways [46, 47]. MAP1B, one of microtubule-associated proteins (MAPs), is reported as the most significant upregulated gene in urothelial carcinoma progression [31]. And phosphorylation of MAP1B associate

with drug sensitive in human glioblastoma [48]. SPOCD1 could inhibits cell apoptosis through PI3K/AKT pathway and accelerates ovarian cancer progression [49]. However, DOK7 and FKBP10 have not been reported as predictor of BLCA patients. Because of DOK7 could inhibit breast cancer cell invasion and migration ability via PI3K/PTEN/AKT pathway, and our result showed a similar pathway. Based on that found, we thought that DOK7 may also could prompt or inhibit bladder cancer. According to the data of TCGA and HPA, the higher expression of DOK7 indicated a bad prognosis, and the results were consistent with our prognostic model. To further verify the functions of DOK7 in bladder cancer, we used siRNA to knockdown the expression of DOK7. Consistently, with the knockdown of DOK7, bladder cancer cell proliferation and migration abilities were promoted.

In consideration of the powerful inflammatory, we explored the correlation between TME and the risk score. Our result showed the high-risk group has a considerably higher StromalScore, ImmuneScore and ESTIMATEScore, indicating that their tumor purity was lower and may associated with poor prognosis [50]. In addition, the fractions of activated CD4 memory T cell, M0, M1 and M2 Macrophages were significantly higher in the high-risk group, while memory B cells, CD8 T cells, naïve CD4 T cells, Tfh, Tregs, monocytes, resting and activated dendritic cells were significantly higher in the low-risk group. Several research reported that the infiltration of memory B cells, CD8 T cells DCs, and Tfh cells in tumor may associate with better prognosis [51–54], while M2 macrophage infiltration correlates with chemotherapy resistance and is associated with a poor prognosis in most cancers [55, 56]. Besides, monocytes also could activate antigen-presenting cells to play a role of antitumor effectors [57]. Other study report Tregs could promote tumor progression by form an immunosuppressive microenvironment [58]. But in our study memory B cells with high components of the TME and CD4 memory T cell with low components of the TME are mean poor prognosis. The conflict requires further investigation in order to be fully understood.

Gene mutations play a critical part in the development of BLCA, and somatic mutations are considered the primary drivers of antitumor adaptive immune response [59]. Our study demonstrated BLCA patients with higher TMB have a better OS survival probability. We also combine risk score and TMB to predict the OS of BLCA patients, and the result show that BLCA patients with low-risk score and high TMB have the greatest OS survival probability. Immune checkpoint inhibitors (ICIs) efficacy are reported have a correlation with TMB, and cancer patients with high TMB seem like to have better reaction to ICIs [60, 61]. Next, we assessed the prognostic model's ability to predict chemotherapy and immunotherapy drug benefit in BLCA patients. The result showed that compared with the low-risk group, doxorubicin, docetaxel, cisplatin, tipifarnib, sunitinib, sorafenib and pazopanib were significantly benefit in the high-risk group. When taken as a whole, the prognostic model may provide better therapy strategies for BLCA patients.

There are still some limits to our research. First, the samples are constrained because of sample size and sample origin from public datasets. Second, the prognostic model needs clinical studies to confirm its accuracy and stability. Moreover, RNA expression is not completely present protein level. As a result, more research is required to overcome these limitations.

Conclusion

In summary, our research identifies a novel prognostic model for predicting prognosis of BLCA patients. Based on our prognostic model, we believe that we could make an accurate judgment based on the different conditions of bladder cancer patients and could provide references for individualized treatment of chemotherapy and immunotherapy drugs.

Acknowledgements

We are truly grateful to the TCGA, GEO and HPA for the contribution of the data.

Author contributions

This document is conceptualized and designed by BS, YY, and DY. Data collection, data analysis, and manuscript writing are all done by ZW, YY, JC, PT, and XC. All of the figures are created by WZ, DY and HZ. CY and SL give study guidance and help to edit the text. The project is supervised and edited by BS, YY, and DY. The final manuscript is read and approved by all of the authors. The essay is co-authored by all writers, who all give their approval to the final edition.

Funding

This work is supported by the National Natural Science Foundation (92059112 and 82072821) and the Shanghai Songjiang Municipal Science and Technology Commission Natural Science Foundation (20SJKJGG250).

Availability of data and materials

The datasets supporting the conclusions of this article are available in The Cancer Genome Atlas database (https://portal.gdc.cancer. gov/), the GEO database (https://www.ncbi.nlm.nih.gov/geo/) and HPA (http://www.proteinatlas.org).

Declarations

Ethics approval and consent to participate

Not applicable.

Consent for publication

Not applicable.

Competing interests

The authors state that there are no commercial or financial relationships that might be considered as a potential conflict of interest during the research.

Received: 12 October 2022 Accepted: 9 January 2023
Published online: 28 January 2023

References

1. Siegel RL, Miller KD, Fuchs HE, Jemal A. Cancer statistics, 2022. CA Cancer J Clin. 2022;72(1):7–33.
2. Witjes JA, Bruins HM, Cathomas R, Comperat EM, Cowan NC, Gakis G, et al. European Association of Urology guidelines on muscle-invasive and metastatic bladder cancer: summary of the 2020 guidelines. Eur Urol. 2021;79(1):82–104.
3. Plimack ER, Bellmunt J, Gupta S, Berger R, Chow LQ, Juco J, et al. Safety and activity of pembrolizumab in patients with locally advanced or metastatic urothelial cancer (KEYNOTE-012): a non-randomised, open-label, phase 1b study. Lancet Oncol. 2017;18(2):212–20.
4. Alfred Witjes J, Lebret T, Comperat EM, Cowan NC, De Santis M, Bruins HM, et al. Updated 2016 EAU Guidelines on muscle-invasive and metastatic bladder cancer. Eur Urol. 2017;71(3):462–75.
5. Angus L, Smid M, Wilting SM, van Riet J, Van Hoeck A, Nguyen L, et al. The genomic landscape of metastatic breast cancer highlights changes in mutation and signature frequencies. Nat Genet. 2019;51(10):1450–8.
6. Dyrskjot L, Ingersoll MA. Biology of nonmuscle-invasive bladder cancer: pathology, genomic implications, and immunology. Curr Opin Urol. 2018;28(6):598–603.
7. Christofferson DE, Yuan J. Necroptosis as an alternative form of programmed cell death. Curr Opin Cell Biol. 2010;22(2):263–8.
8. Degterev A, Hitomi J, Germscheid M, Ch'en IL, Korkina O, Teng X, et al. Identification of RIP1 kinase as a specific cellular target of necrostatins. Nat Chem Biol. 2008;4(5):313–21.
9. Vandenabeele P, Galluzzi L, Vanden Berghe T, Kroemer G. Molecular mechanisms of necroptosis: an ordered cellular explosion. Nat Rev Mol Cell Biol. 2010;11(10):700–14.
10. Rosenbaum DM, Degterev A, David J, Rosenbaum PS, Roth S, Grotta JC, et al. Necroptosis, a novel form of caspase-independent cell death, contributes to neuronal damage in a retinal ischemia-reperfusion injury model. J Neurosci Res. 2010;88(7):1569–76.
11. Kaczmarek A, Vandenabeele P, Krysko DV. Necroptosis: the release of damage-associated molecular patterns and its physiological relevance. Immunity. 2013;38(2):209–23.
12. Gong Y, Fan Z, Luo G, Yang C, Huang Q, Fan K, et al. The role of necroptosis in cancer biology and therapy. Mol Cancer. 2019;18(1):100.
13. Koo GB, Morgan MJ, Lee DG, Kim WJ, Yoon JH, Koo JS, et al. Methylation-dependent loss of RIP3 expression in cancer represses programmed necrosis in response to chemotherapeutics. Cell Res. 2015;25(6):707–25.
14. Li X, Guo J, Ding AP, Qi WW, Zhang PH, Lv J, et al. Association of mixed lineage kinase domain-like protein expression with prognosis in patients with colon cancer. Technol Cancer Res Treat. 2017;16(4):428–34.
15. Wu W, Zhu H, Fu Y, Shen W, Xu J, Miao K, et al. Clinical significance of down-regulated cylindromatosis gene in chronic lymphocytic leukemia. Leuk Lymphoma. 2014;55(3):588–94.
16. Colbert LE, Fisher SB, Hardy CW, Hall WA, Saka B, Shelton JW, et al. Pronecrotic mixed lineage kinase domain-like protein expression is a prognostic biomarker in patients with early-stage resected pancreatic adenocarcinoma. Cancer. 2013;119(17):3148–55.
17. Wang Q, Chen W, Xu X, Li B, He W, Padilla MT, et al. RIP1 potentiates BPDE-induced transformation in human bronchial epithelial cells through catalase-mediated suppression of excessive reactive oxygen species. Carcinogenesis. 2013;34(9):2119–28.
18. Johnstone RW, Ruefli AA, Lowe SW. Apoptosis: a link between cancer genetics and chemotherapy. Cell. 2002;108(2):153–64.
19. Casagrande N, Borghese C, Favero A, Vicenzetto C, Aldinucci D. Trabectedin overcomes doxorubicin-resistance, counteracts tumor-immunosuppressive reprogramming of monocytes and decreases xenograft growth in Hodgkin lymphoma. Cancer Lett. 2021;500:182–93.
20. Wang KJ, Meng XY, Chen JF, Wang KY, Zhou C, Yu R, et al. Emodin induced necroptosis and inhibited glycolysis in the renal cancer cells by enhancing ROS. Oxid Med Cell Longev. 2021;2021:8840590.
21. Yatim N, Jusforgues-Saklani H, Orozco S, Schulz O, Barreira da Silva R, Reis e Sousa C, et al. RIPK1 and NF-kappaB signaling in dying cells determines cross-priming of CD8+ T cells. Science. 2015;350(6258):328–34.
22. Snyder AG, Hubbard NW, Messmer MN, Kofman SB, Hagan CE, Orozco SL, et al. Intratumoral activation of the necroptotic pathway components RIPK1 and RIPK3 potentiates antitumor immunity. Sci Immunol. 2019;4(36):eaaw2004.
23. Irizarry RA, Hobbs B, Collin F, Beazer-Barclay YD, Antonellis KJ, Scherf U, et al. Exploration, normalization, and summaries of high density oligonucleotide array probe level data. Biostatistics. 2003;4(2):249–64.
24. Xin S, Mao J, Duan C, Wang J, Lu Y, Yang J, et al. Identification and quantification of necroptosis landscape on therapy and prognosis in kidney renal clear cell carcinoma. Front Genet. 2022;13:832046.
25. Thul PJ, Akesson L, Wiking M, Mahdessian D, Geladaki A, Ait Blal H, et al. A subcellular map of the human proteome. Science. 2017;356(6340):eaal3321.
26. Wilkerson MD, Hayes DN. ConsensusClusterPlus: a class discovery tool with confidence assessments and item tracking. Bioinformatics. 2010;26(12):1572–3.
27. Zhang J, Xi J, Huang P, Zeng S. Comprehensive analysis identifies potential ferroptosis-associated mRNA therapeutic targets in ovarian cancer. Front Med (Lausanne). 2021;8:644053.
28. Kanehisa M, Furumichi M, Tanabe M, Sato Y, Morishima K. KEGG: new perspectives on genomes, pathways, diseases and drugs. Nucleic Acids Res. 2017;45(D1):D353–61.
29. Newman AM, Liu CL, Green MR, Gentles AJ, Feng W, Xu Y, et al. Robust enumeration of cell subsets from tissue expression profiles. Nat Methods. 2015;12(5):453–7.
30. Li P, Li L, Li Z, Wang S, Li R, Zhao W, et al. Annexin A1 promotes the progression of bladder cancer via regulating EGFR signaling pathway. Cancer Cell Int. 2022;22(1):7.
31. Chien TM, Chan TC, Huang SK, Yeh BW, Li WM, Huang CN, et al. Role of microtubule-associated protein 1b in urothelial carcinoma: overexpression predicts poor prognosis. Cancers (Basel). 2020;12(3):630.
32. van der Heijden AG, Mengual L, Lozano JJ, Ingelmo-Torres M, Ribal MJ, Fernandez PL, et al. A five-gene expression signature to predict progression in T1G3 bladder cancer. Eur J Cancer. 2016;64:127–36.
33. Wang J, Zhang C, Wu Y, He W, Gou X. Identification and analysis of long non-coding RNA related miRNA sponge regulatory network in bladder urothelial carcinoma. Cancer Cell Int. 2019;19:327.
34. Yue C, Bai Y, Piao Y, Liu H. DOK7 inhibits cell proliferation, migration, and invasion of breast cancer via the PI3K/PTEN/AKT pathway. J Oncol. 2021;2021:4035257.
35. Yan Y, Cai J, Huang Z, Cao X, Tang P, Wang Z, et al. A novel ferroptosis-related prognostic signature reveals macrophage infiltration and EMT status in bladder cancer. Front Cell Dev Biol. 2021;9:712230.
36. Yan Y, Cao X, Wang Z, Huang Z, Cai J, Tang P, et al. Pyroptosis-related patterns predict tumor immune landscape and immunotherapy response in bladder cancer. Front Mol Biosci. 2022;9:815290.
37. Yang R, Zhang W, Shang X, Chen H, Mu X, Zhang Y, et al. Neutrophil-related genes predict prognosis and response to immune checkpoint inhibitors in bladder cancer. Front Pharmacol. 2022;13:1013672.
38. Feng ZH, Liang YP, Cen JJ, Yao HH, Lin HS, Li JY, et al. m6A-immune-related lncRNA prognostic signature for predicting immune landscape and prognosis of bladder cancer. J Transl Med. 2022;20(1):492.
39. Zou W, Wolchok JD, Chen L. PD-L1 (B7–H1) and PD-1 pathway blockade for cancer therapy: mechanisms, response biomarkers, and combinations. Sci Transl Med. 2016;8(328):328rv4.
40. Iglesias JM, Morgan RO, Jenkins NA, Copeland NG, Gilbert DJ, Fernandez MP. Comparative genetics and evolution of annexin A13 as the founder gene of vertebrate annexins. Mol Biol Evol. 2002;19(5):608–18.
41. Han PF, Che XD, Li HZ, Gao YY, Wei XC, Li PC. Annexin A1 involved in the regulation of inflammation and cell signaling pathways. Chin J Traumatol. 2020;23(2):96–101.
42. Yu S, Meng Q, Hu H, Zhang M. Correlation of ANXA1 expression with drug resistance and relapse in bladder cancer. Int J Clin Exp Pathol. 2014;7(9):5538–48.
43. Bergamin E, Hallock PT, Burden SJ, Hubbard SR. The cytoplasmic adaptor protein Dok7 activates the receptor tyrosine kinase MuSK via dimerization. Mol Cell. 2010;39(1):100–9.

44. Yang SM, Li SY, Yu HB, Li JR, Sun LL. Repression of DOK7 mediated by DNMT3A promotes the proliferation and invasion of KYSE410 and TE-12 ESCC cells. Biomed Pharmacother. 2017;90:93–9.
45. Heyn H, Carmona FJ, Gomez A, Ferreira HJ, Bell JT, Sayols S, et al. DNA methylation profiling in breast cancer discordant identical twins identifies DOK7 as novel epigenetic biomarker. Carcinogenesis. 2013;34(1):102–8.
46. Cai HQ, Zhang MJ, Cheng ZJ, Yu J, Yuan Q, Zhang J, et al. FKBP10 promotes proliferation of glioma cells via activating AKT-CREB-PCNA axis. J Biomed Sci. 2021;28(1):13.
47. Chen Z, He L, Zhao L, Zhang G, Wang Z, Zhu P, et al. circREEP3 drives colorectal cancer progression via activation of FKBP10 transcription and restriction of antitumor immunity. Adv Sci (Weinh). 2022;9(13):e2105160.
48. Laks DR, Oses-Prieto JA, Alvarado AG, Nakashima J, Chand S, Azzam DB, et al. A molecular cascade modulates MAP1B and confers resistance to mTOR inhibition in human glioblastoma. Neuro Oncol. 2018;20(6):764–75.
49. Liu D, Yang Y, Yan A, Yang Y. SPOCD1 accelerates ovarian cancer progression and inhibits cell apoptosis via the PI3K/AKT pathway. Onco Targets Ther. 2020;13:351–9.
50. Zeng D, Zhou R, Yu Y, Luo Y, Zhang J, Sun H, et al. Gene expression profiles for a prognostic immunoscore in gastric cancer. Br J Surg. 2018;105(10):1338–48.
51. Seifert M, Kuppers R. Human memory B cells. Leukemia. 2016;30(12):2283–92.
52. Farhood B, Najafi M, Mortezaee K. CD8(+) cytotoxic T lymphocytes in cancer immunotherapy: a review. J Cell Physiol. 2019;234(6):8509–21.
53. Yoshitomi H, Ueno H. Shared and distinct roles of T peripheral helper and T follicular helper cells in human diseases. Cell Mol Immunol. 2021;18(3):523–7.
54. Wculek SK, Cueto FJ, Mujal AM, Melero I, Krummel MF, Sancho D. Dendritic cells in cancer immunology and immunotherapy. Nat Rev Immunol. 2020;20(1):7–24.
55. Lan J, Sun L, Xu F, Liu L, Hu F, Song D, et al. M2 macrophage-derived exosomes promote cell migration and invasion in colon cancer. Cancer Res. 2019;79(1):146–58.
56. Cassetta L, Pollard JW. Targeting macrophages: therapeutic approaches in cancer. Nat Rev Drug Discov. 2018;17(12):887–904.
57. Ugel S, Cane S, De Sanctis F, Bronte V. Monocytes in the tumor microenvironment. Annu Rev Pathol. 2021;16:93–122.
58. Ohue Y, Nishikawa H. Regulatory T (Treg) cells in cancer: can Treg cells be a new therapeutic target? Cancer Sci. 2019;110(7):2080–9.
59. Lawson ARJ, Abascal F, Coorens THH, Hooks Y, O'Neill L, Latimer C, et al. Extensive heterogeneity in somatic mutation and selection in the human bladder. Science. 2020;370(6512):75–82.
60. Buttner R, Longshore JW, Lopez-Rios F, Merkelbach-Bruse S, Normanno N, Rouleau E, et al. Implementing TMB measurement in clinical practice: considerations on assay requirements. ESMO Open. 2019;4(1):e000442.
61. Samstein RM, Lee CH, Shoushtari AN, Hellmann MD, Shen R, Janjigian YY, et al. Tumor mutational load predicts survival after immunotherapy across multiple cancer types. Nat Genet. 2019;51(2):202–6.

Publisher's Note